Alternating synchronizability of complex clustered networks with regular local structure

Liang Huang,[1] Ying-Cheng Lai,[1,2] and Robert A. Gatenby[3]
[1]*Department of Electrical Engineering, Arizona State University, Tempe, Arizona 85287, USA*
[2]*Department of Physics and Astronomy, Arizona State University, Tempe, Arizona 85287, USA*
[3]*Department of Radiology and Department of Applied Mathematics, University of Arizona, Tucson, Arizona 85721, USA*
(Received 15 May 2007; revised manuscript received 14 November 2007; published 14 January 2008)

Small network distance and homogeneous degree distribution have been found to be critical to efficient network synchronization. In this paper, we investigate the synchronizability of clustered networks with regular subnetworks and report a counterintuitive phenomenon: As the density of intracluster links is increased, the network exhibits strong and weak synchronizability in an alternating manner. A theory based on analyzing the eigenvalues and eigenvectors of the coupling matrix is provided to explain this phenomenon. The relevance of the network model to tissue organization for intercellular communication in biological systems is discussed. An implication is that, in order to achieve synchronization, local coupling density in the network needs to be tuned properly.

DOI: 10.1103/PhysRevE.77.016103 PACS number(s): 89.75.Hc, 87.18.Hf, 05.45.Xt, 87.10.−e

I. INTRODUCTION

Synchronization in complex networks has attracted much attention recently [1–7]. Earlier works have found that random [8], small-world [9], and scale-free [10] networks, due to their small network distances, are generally more synchronizable than regular networks [1]. However, small network distance alone is not a guarantee for strong synchronizability. For example, for a scale-free network, the existence of hubs contributes to a small network distance but the underlying heterogeneous degree distribution can cause a wide spread in the eigenvalues of the coupling matrix, which can actually inhibit network synchronization [2]. More recent works have found that, by assigning larger weights to the hubs or introducing a gradient field from hub nodes to small degree nodes, scale-free networks can be more synchronizable than random networks [3]. Modifying local connecting structure, if done properly, can also change the synchronizability significantly [4]. Synchronizability of complex clustered networks has begun to be investigated only recently [5–7].

In this paper, we investigate the synchronizability of locally regular, complex clustered networks (see Sec. II for motivations from systems biology). A clustered network consists of a number of groups, where nodes within each group are densely connected, but the linkages among the groups are sparse. In fact, the tendency to form a clustered network structure appears to be a key organizational feature in biological systems, such as protein-protein interaction networks [11–13] and metabolic graphs [14]. Previous works have also revealed that the clustered topology is fundamental to many types of social and technological networks [15]. Our recent work [7] on the synchronizability of clustered networks with *random* subnetworks has revealed an interesting phenomenon, namely, more links, which make the network smaller, do not necessarily lead to a stronger synchronizability. There can be situations where extra links, if placed improperly, can suppress synchronization. Realistic considerations stipulate that the globally random connections among clusters be sparse. Thus a key question is what can happen to network synchronizability when the density of intracluster links is varied. We find that, for a typical locally regular clustered network, its synchronizability exhibits an alternating, highly nonmonotonic behavior as a function of the intracluster link density. In fact, there are distinct regions of the density for which the network synchronizability is maximized, but there are also parameter regions in between for which the synchronizability diminishes. We show that, while surprising, this phenomenon of *alternating synchronizability* can be fully explained theoretically based on analyzing the behavior of the eigenvalues and eigenvectors of the coupling matrix. A feature that makes our theoretical analysis feasible is that, due to the locally regular topology of the network, some key eigenvectors within each individual cluster exhibit periodic wave patterns. Both numerical eigenvalue calculations and direct simulation of the actual synchronization dynamics of the underlying oscillator network provide firm support for the theory. One implication is that, in order to achieve robust synchronization, the density of the local connections within a cluster needs to be appropriately tuned since both high density and low density can hinder synchronization.

Considerations from systems biology that motivate our work are described in Sec. II. A detailed theoretical treatment of the synchronizabilities of clustered networks with regular subnetworks is provided in Sec. III. In particular, we begin with relatively simple networks of two clusters and then extend the analysis to networks with multiple clusters. The issue of robustness of the alternating-synchronization behavior will also be addressed. Direct numerical support from actual simulations of synchronous dynamics is provided in Sec. IV. Discussions are presented in Sec. V.

II. BIOLOGICAL MOTIVATIONS

Complex multicellular organisms such as the human body require multiscale organizational structures, including formation of organs from large numbers of cells and integration of many organs into the systemic structure necessary for individual survival and proliferation. The organs typically consist of large numbers of multicellular functional units such as crypt in the colon, nephron in the kidney, lobule in the liver,

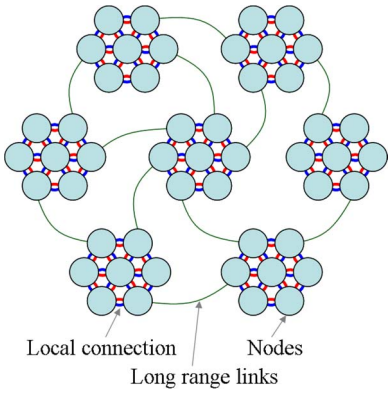

FIG. 1. (Color online) Schematic illustration of our clustered network model with regular subnetworks.

and alveolus in the lung, etc. While extensive recent work has focused on the structure and dynamics of intracellular molecular networks [16–20], there has been little effort to extend this kind of analysis to the interactions among cells within functioning multicellular organs which allow, for example, the human liver to synchronize as many as 10^{12} individual cells into a single functioning unit. There are two general methods by which cells can communicate with each other. Locally, cells usually establish their mutual communication channels through transmembrane pathways such as gap junctions that allow small molecules to pass between two cells in both directions. At a larger scale, cells communicate with each other through diffusing signals with cell-specific receptors. The interaction is usually directed in the sense that signals such as growth factors are produced by some, but not all cells, and can be received only by other cells that express the appropriate receptors. Despite the fact that many of the specific pathways by which cells communicate have been reasonably well characterized, remarkably little is known about the organizational principles that govern communications among large numbers of cells and permit synchronized function over substantial distances [21,22].

Since cells communicate with each other using the two general methods described above, an intercellular-information network contains two essential features: A *locally regular* topology based on local communication with neighbors via membrane structures such as gap junction and integrins [23] and *globally random*, directional couplings based on long-range diffusing signals and the corresponding cell membrane receptors. To better distinguish between local and global interactions, it is useful to assume that local interactions are confined within clusters, and global interactions occur among the clusters, as shown in Fig. 1. The result is a class of complex clustered networks with a regular subnetwork in each cluster but with random, sparse couplings among clusters. We shall address the issue of synchronization on this class of networks. This is reasonable because there are two basic biological requirements for such a network: (1) There must be a sufficient degree of synchronization to permit the entire organ to function as a single unit, so as new cells are "added" during growth and repair, their precise locations and differentiated phenotypes are specified with nearly perfect accuracy; and (2) the synchronization must be robust so that lost cells (due, for example, to a wound) can be replaced and the system is resistant to cascading failure, enabling isolation of infections such as viruses to prevent rapid, global spread.

III. SYNCHRONIZABILITY VIA SPECTRAL ANALYSIS

We consider the following network structure: N nodes are grouped into M clusters, where each cluster contains $n=N/M$ nodes. In each cluster, the nodes are ordered on a ring so that the subnetwork is regular. Each node connects to m nearest neighbors. Each pair of nodes in different clusters is connected with probability p. While biological considerations stipulate that the long-range links, i.e., links between clusters, be directional, to be as general as possible we shall treat both bidirectional and directional coupling cases. To facilitate analytic derivation and understanding, we first consider a network consisting of two clusters with bidirectional intercluster links and then generalize the theory to M-cluster networks for $M>2$.

The standard approach to addressing the synchronizability of a complex network is to consider a corresponding coupled oscillator network [1], where one nonlinear oscillator is placed on each node of the network. The dynamical system can be described by

$$\frac{d\mathbf{x}_i}{dt} = \mathbf{F}(\mathbf{x}_i) - \epsilon \sum_{j=1}^{N} G_{ij}\mathbf{H}(\mathbf{x}_j), \quad i = 1,2,\ldots,N, \tag{1}$$

where ϵ is a global coupling parameter, $\mathbf{G}$ is the coupling matrix determined by the network topology, and $\mathbf{H}(\mathbf{x})$ is a coupling function. The coupling matrix $\mathbf{G}$ is defined as $G_{ij}=-1/k_i$ if there is a link between node i and j, where k_i is the degree (the number of links) of node i, $G_{ii}=1$, and $G_{ij}=0$ otherwise. For a bidirectional network, the eigenvalues of $\mathbf{G}$ are real and non-negative, and can be sorted as $0=\lambda_1<\lambda_2 \leq \cdots \leq \lambda_N$ [24]. The coupled system is synchronizable only if the effective coupling strength $K=\epsilon\lambda_i$ $(i>1)$ falls into a certain interval (K_1,K_2), or $K_1<\epsilon\lambda_2$ and $K_2>\epsilon\lambda_N$, where K_1 and K_2 depend only on the dynamics of a single oscillator [25]. For typical oscillators the second condition can be easily satisfied, so the synchronization condition is $\lambda_2>K_1/\epsilon$ [7]. The goal of our analysis is to derive a formula for λ_2 for clustered networks with a regular local structure.

A. Networks with two clusters

The transpose of a matrix and the matrix itself have the same set of eigenvalues. Let $\mathbf{e}_i$ be the normalized eigenvector such that $\mathbf{G}^T\cdot\mathbf{e}_i=\lambda_i\mathbf{e}_i$, where $[*]^T$ denotes the transpose. Since $\Sigma_j G_{ij}=0$, we have $\Sigma_j e_{i,j}=0$ if $\lambda_i\neq 0$ [26]. It is known that for a one-dimensional ring network, the eigenvector $\mathbf{e}_2$ associated with λ_2 has a sinusoidal waveform: $e_{2,i} \sim \sin(2\pi i/n)$, where n is the total number of nodes on the ring. For two coupled ring subnetworks, we find numerically that, when the inter- and intraconnections are not too dense, components in $\mathbf{e}_2$ have a similar wave pattern for each subnetwork, although the mean values can be different, as shown in Fig. 2. Since the two subnetworks are identical, the

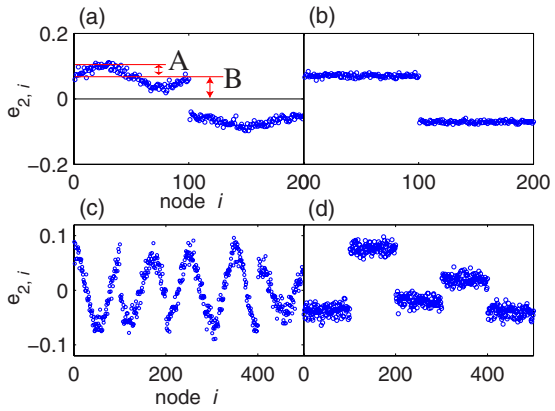

FIG. 2. (Color online) Typical configurations of $\mathbf{e}_2$ for a two-cluster network of parameters $N=200$ and $p=0.2$ [(a) $m=52$ and (b) $m=80$] and for a five-cluster network with $N=500$ and $p=0.3$ [(c) $m=40$ and (d) $m=80$].

amplitudes of the periodic waves are the same. The zero-sum property of $\mathbf{e}_2$ requires that the mean values of the two sinusoidal waves have opposite signs. To characterize such a wave pattern, we define A to be the amplitude of the sinusoidal waves, and B as the positive mean value, as indicated in Fig. 2(a). Thus $\mathbf{e}_2$ can be written approximately as

$$\mathbf{e}_2 = [\{B + A\sin(2\pi i_1/n + \phi_1)\}_{i_1}, \{-B + A\sin(2\pi i_2/n + \phi_2)\}_{i_2}]^T,$$

where $i_1, i_2 = 1, 2, \ldots, n$, and ϕ_1 and ϕ_2 are the phases of the first node in each cluster. We can relabel the nodes so that $\phi_1 = \phi_2 = 0$, thus have

$$\mathbf{e}_2 = [\{B + A\sin(2\pi i_1/n)\}_{i_1}, \{-B + A\sin(2\pi i_2/n)\}_{i_2}]^T.$$

The normalization condition $\mathbf{e}_2^T\mathbf{e}_2 = 1$ gives

$$\sum_{i_1=1}^{n}\left[B + A\sin\left(\frac{2\pi i_1}{n}\right)\right]^2 + \sum_{i_2=1}^{n}\left[-B + A\sin\left(\frac{2\pi i_2}{n}\right)\right]^2 = 1,$$

which yields

$$2nB^2 + nA^2 = 1. \quad (2)$$

For a network whose $\mathbf{e}_2$ has a periodic wave pattern in each cluster, the corresponding eigenvalue λ_2 can be calculated *analytically*. Likewise, if $\mathbf{e}_2$ is constant within each cluster, λ_2 can be obtained analytically as well [7]. The key observation is that, as the intracluster link density is increased, there is a transition from the former to the latter. That is, there exists a critical value m_t, where for $m < m_t$, the eigenvector $\mathbf{e}_2$ possesses a periodic wave pattern in each cluster but, for $m > m_t$, $\mathbf{e}_2$ is approximately constant in each cluster. Our effort below will then be to obtain m_t, based on which the eigenvalue λ_2 can be calculated.

To proceed, we note that, from the definition $\mathbf{G}^T\cdot\mathbf{e}_2 = \lambda_2\mathbf{e}_2$, we have

$$\lambda_2 = \mathbf{e}_2^T\cdot\mathbf{G}^T\cdot\mathbf{e}_2 = \sum_{i,j=1}^{N} G_{ij}e_{2,i}e_{2,j}.$$

The coupling matrix $\mathbf{G}$ has the structure that, for $i - m/2 \le j < i$ and $i < j \le i + m/2$, $G_{ij} = -1/k_i$, and for j belonging to different clusters, $G_{ij} = -1/k_i$ with probability p. The degree k_i follows approximately a Gaussian distribution: $P(k) \sim N(m+pn, \sqrt{pn})$; thus we can use the mean value $k \equiv m + pn$ to approximate k_i. As a result, λ_2 can be expanded as

$$\lambda_2 = \sum_{i_1=1}^{n}\left[B + A\sin\left(\frac{2\pi i_1}{n}\right)\right]\left\{\left[B + A\sin\left(\frac{2\pi i_1}{n}\right)\right] - \frac{1}{k}\sum_{l=-m/2, l\neq 0}^{m/2}\left[B + A\sin\left(\frac{2\pi(i_1+l)}{n}\right)\right] + \sum_{i_2=1}^{n} G_{i_1(n+i_2)} \times\left[-B + A\sin\left(\frac{2\pi i_2}{n}\right)\right]\right\} + \text{c.c.},$$

where c.c. stands for the summation for the second cluster, i.e., with i_1 and $n+i_2$ interchanged. Since the clusters are identical, the two summations are the same. The first term in the summation for the first cluster, which is $\mathbf{e}_2^T\cdot\mathbf{e}_2/2$, gives $1/2$. For the third term, note that $G_{i_1(n+i_2)}$ equals $-1/k$ with probability p. Because of this randomness, the summation over $A\sin(2\pi i_2/n)$ vanishes, and

$$\sum_{i_1=1}^{n}[B + A\sin(2\pi i_1/n)] = nB.$$

Thus the third term equals $nB(-1/k)np(-B) = n^2pB^2/k$. The second term, when expanded, gives

$$-\frac{1}{k}\left\{\sum_{i_1=1}^{n}\left[B + A\sin\left(\frac{2\pi i_1}{n}\right)\right]\sum_{l=-m/2}^{m/2}\left[B + A\sin\left(\frac{2\pi(i_1+l)}{n}\right)\right] - \sum_{i_1=1}^{n}\left[B + A\sin\left(\frac{2\pi i_1}{n}\right)\right]^2\right\}.$$

Since

$$\sum_{i_1=1}^{n}\sum_{l=-m/2}^{m/2}\sin\frac{2\pi(i_1+l)}{n} = \sum_{l=-m/2}^{m/2}\sum_{i_1=1}^{n}\sin\frac{2\pi(i_1+l)}{n} = 0,$$

the second term can be simplified as

$$-\frac{1}{k}\left\{n(m+1)B^2 + A^2\sum_{i_1=1}^{n}\sin\left(\frac{2\pi i_1}{n}\right)\times\sum_{l=-m/2}^{m/2}\sin\left[\frac{2\pi(i_1+l)}{n}\right] - \frac{1}{2}\right\} \approx -\frac{1}{k}\left\{n(m+1)B^2 - \frac{1}{2} + A^2\int_0^n\sin\left(\frac{2\pi x}{n}\right)dx\int_{-m/2}^{m/2}\sin\left[\frac{2\pi(x+y)}{n}\right]dy\right\}$$

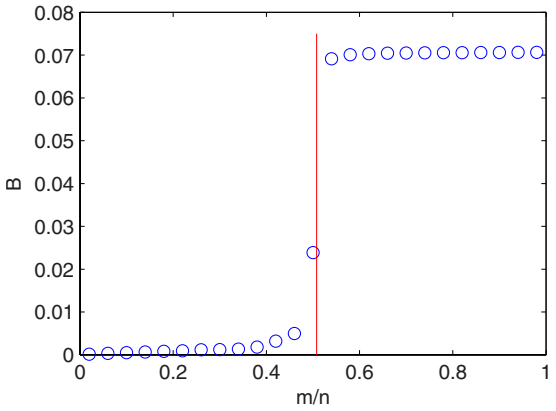

FIG. 3. (Color online) For a two-cluster network with $N=200$, and $p=0.2$, quantity B vs m/n from simulation, where each point is the average of 100 runs. For $m/n>0.5$, B approaches $1/\sqrt{N} \simeq 0.071$. The vertical line indicating the transition point of B is predicted by theory.

$$= -\frac{1}{k}\left\{ n(m+1)B^2 - \frac{1}{2} + \frac{n^2A^2}{2\pi}\sin\frac{\pi m}{n} \right\}$$
$$= -\frac{1}{k}\left\{ nmB^2 + \frac{nA^2}{2}\left[\frac{n}{\pi}\sin\frac{\pi m}{n} - 1 \right] \right\},$$

where the last equality is due to Eq. (2). Adding all the three terms, we have

$$\lambda_2 = 2\left\{ \frac{1}{2} + \frac{n^2pB^2}{k} - \frac{nmB^2}{k} - \frac{nA^2}{2k}\left[\frac{n}{\pi}\sin\frac{\pi m}{n} - 1 \right] \right\}$$
$$= 1 + \frac{2nB^2(np-m)}{k} - \frac{NA^2}{2k}\left[\frac{n}{\pi}\sin\frac{\pi m}{n} - 1 \right]. \quad (3)$$

While the parameter A represents the magnitude of the waveform, B can be regarded as the strength of the clustering of the network. Figure 3 shows the value of B versus m/n. There is a sudden transition of B from 0 to $1/\sqrt{N}$ (or correspondingly, A from $\sqrt{2/N}$ to 0). Thus we can approximate B (or A) by a step function of m/n. The transition point m_t where the wave patterns vanish (A becomes 0) can be calculated, as follows. For $B=0$, we have $A=\sqrt{2/N}$ and Eq. (3) becomes

$$\lambda_2 = 1 - \frac{1}{k}\left(\frac{n}{\pi}\sin\frac{\pi m}{n} - 1 \right). \quad (4)$$

For $B=1/\sqrt{N}$, we have $A=0$. Noting that $k=(N-n)p+m$, we can simplify Eq. (3) as

$$\lambda_2 = 1 + \frac{np-m}{k} = \frac{Np}{k}. \quad (5)$$

Since λ_2 is continuous, at the transition point m_t, the values of λ_2 obtained from Eq. (4) and from Eq. (5) must be equal. This yields

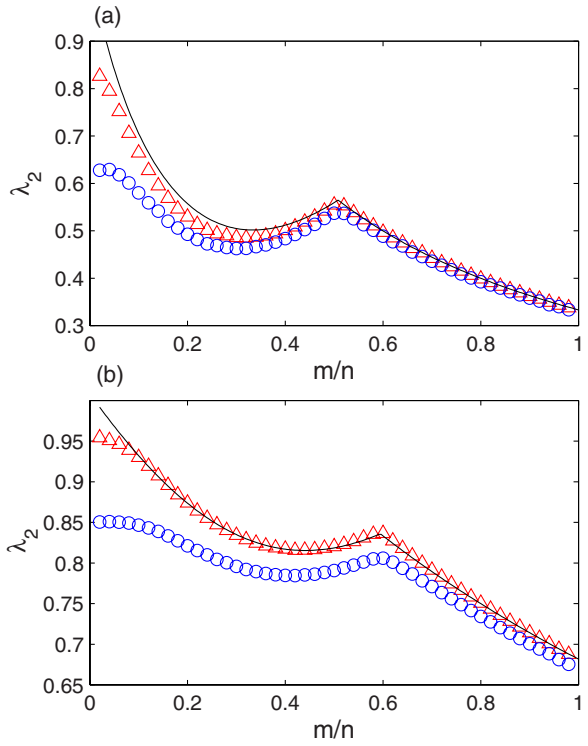

FIG. 4. (Color online) (a) For a two-cluster network with $N=200$ and $p=0.2$ and (b) a five-cluster network with $N=500$ and $p=0.3$, λ_2 vs m/n. The data points are obtained from simulation for both bidirectional (circles) and directional (triangles) intercluster connections. For the directional case, only the real part of λ_2 is presented ($\mathrm{Im}\,\lambda_2 \sim 10^{-3}\,\mathrm{Re}\,\lambda_2$). Each point is the average of 100 realizations. Solid curves are from theory.

$$p = \frac{m_t}{n} - \frac{1}{\pi}\sin\frac{\pi m_t}{n} + \frac{1}{n}. \quad (6)$$

For the parameters used in Fig. 3, the transition point is $m_t \approx 0.508$, as indicated by the vertical line. The analytical value agrees well with the simulation result. Thus, for a two-cluster network, λ_2 can be approximated by Eq. (4) for $m < m_t$ and by Eq. (5) for $m \geq m_t$. Figure 4(a) shows simulation results and the theoretical prediction for λ_2 for both the bidirectional (circles) and directional (triangles) intercluster coupling case. There is an alternating behavior in λ_2 as the intracluster link density m/n is increased and the theory captures the behavior of λ_2 reasonably well.

B. Multicluster networks

For a multicluster network, periodic wave patterns can arise in each cluster as well [Fig. 2(c)]. We have observed numerically that the amplitudes of the wave patterns for different clusters are approximately equal, so the average amplitude A can again be used to characterize the wave patterns. Similar to the two-cluster case, there is a sharp transition of A from a constant value to zero as m/n increases. For $A=0$, the wave pattern diminishes, and $\mathbf{e}_2$ has the structure that its components within one cluster have approximately the same value but they can vary significantly in different clusters [Fig. 2(d)]. In this case, it can be shown that λ_2 is given by

Eq. (5) [7]. To treat the case where $A \neq 0$, we assume the network has M clusters. The eigenvector $\mathbf{e}_2$ has the form of (after relabeling)

$$[\{A \sin(2\pi i_1/n)\}_{i_1}, \ldots, \{A \sin(2\pi i_M/n)\}_{i_M}]^T,$$

for $i_1, \ldots, i_M = 1, 2, \ldots, n$. The normalization condition of $\mathbf{e}_2$ gives $(n/2)A^2M = NA^2/2 = 1$, which yields

$$A = \sqrt{\frac{2}{N}}. \tag{7}$$

Again we have $\lambda_2 = \Sigma_{i,j=1}^{N} G_{ij} e_{2,i} e_{2,j}$. Note that the index $i_1, \ldots, i_M$ are interchangeable; thus we can focus the summation over i on a single cluster and carry out summation over j. Doing so, we find that λ_2 is M times such summations:

$$\lambda_2 = M \sum_{i=1}^{n} A \sin\frac{2\pi i}{n} \left[A \sin\frac{2\pi i}{n} - \frac{1}{k_i} \sum_{l=-m/2, l\neq 0}^{m/2} A \sin\left(\frac{2\pi(i+l)}{n}\right) + \sum_{j \notin V_i} G_{ij} A \sin\left(\frac{2\pi j}{n}\right) \right], \tag{8}$$

where V_i is the set of nodes in the cluster containing i. Since G_{ij} equals $-1/k_i$ with probability p and 0 otherwise, the third term leads to 0. Using the mean value $k \equiv m + p(M-1)n$ to approximate k_i, we have

$$\lambda_2 = M \sum_{i=1}^{n} A \sin\frac{2\pi i}{n} \left\{ \frac{k+1}{k} A \sin\frac{2\pi i}{n} - \frac{1}{k} \sum_{l=-m/2}^{m/2} A \sin\left[\frac{2\pi(i+l)}{n}\right] \right\}$$
$$= \frac{k+1}{k} - M \sum_{i=1}^{n} \frac{1}{k} A \sin\frac{2\pi i}{n} \sum_{l=-m/2}^{m/2} A \sin\left[\frac{2\pi(i+l)}{n}\right].$$

The second term can be approximated by integration, which yields

$$\lambda_2 = \frac{k+1}{k} - \frac{MA^2}{k} \frac{n^2}{2\pi} \sin\frac{\pi m}{n},$$
$$= 1 - \frac{1}{k}\left(\frac{n}{\pi} \sin\frac{\pi m}{n} - 1\right), \tag{9}$$

where the second equality results from using Eq. (7). This expression is the same as Eq. (4) for the two-cluster network case. Since the expressions for λ_2 for both nonzero A and zero A cases are the same as those in the two-cluster case, the transition point m_t can again be determined by Eq. (6), which is independent of M. Thus λ_2 can be approximated by Eq. (4) [or Eq. (9)] for $m < m_t$ and by Eq. (5) for $m \geq m_t$. Figure 4(b) shows the theoretical prediction of λ_2 together with simulation results for a five-cluster network. It can be seen that the alternating behavior in λ_2 persists and is reasonably well predicted by theory.

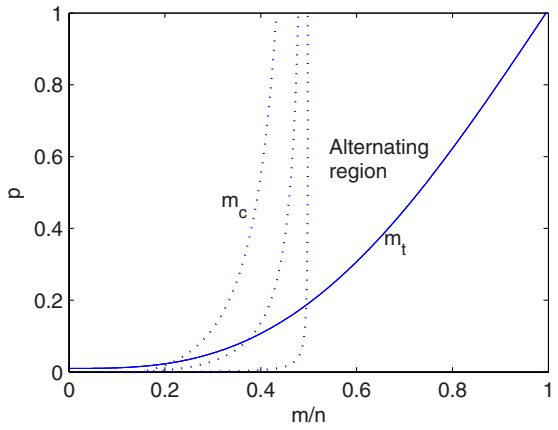

FIG. 5. (Color online) For clustered networks with parameters $M=2$, 5, 100 and $n=100$, p vs m_t/n (solid lines) and vs m_c/n (dotted lines), where three dotted cases from left to right correspond to $M=2,5,100$, respectively. The region between the m_c line and the m_t line, i.e., $m_c < m < m_t$, is the region that λ_2 and therefore the synchronizability exhibit an alternating behavior.

C. Robustness of alternating synchronization behavior

An immediate question is whether the predicted alternating behavior in λ_2 is robust. To address this, we need to determine the value of m_c for which λ_2 in Eq. (4) has a minimum value or $d\lambda_2/dm|_{m_c} = 0$. We obtain

$$p = \left(\frac{\frac{1}{\pi} \sin\frac{\pi m_c}{n} - \frac{1}{n}}{\cos\frac{\pi m_c}{n}} - \frac{m_c}{n} \right) \Bigg/ (M-1). \tag{10}$$

For a given set of parameters (M,n,p), λ_2 is maximized at m_t and reaches minimum at m_c. Thus the system can be synchronized at m_t and desynchronized at m_c. As a result, the alternating behavior exists if $m_c < m_t$. Neglecting the term $1/n$, m_t/n only depends on p [Eq. (6)], while m_c/n depends on both p and M [Eq. (10)]. Figure 5 shows m_c and m_t for different M values. For clarity only one n value is used since the curves for $n=100$ and $n=1000$ are almost identical. For large values of M, for any p, m_c approaches $n/2$. Thus for the particular parameter setting in Fig. 5, insofar as $p > 0.2$, networks with arbitrary number of clusters exhibit the alternating behavior. When M is smaller, the critical value for p for the alternating behavior decreases and the parameter region for the alternating behavior broadens. The conclusion is that the alternating behavior in synchronization is a quite robust feature in locally regular, complex clustered networks.

IV. NUMERICAL SIMULATIONS OF ACTUAL SYNCHRONOUS DYNAMICS

While the alternating-synchronizability behavior is predicted and verified using eigenvalue analysis, direct numerical simulations of coupled oscillator networks give strong

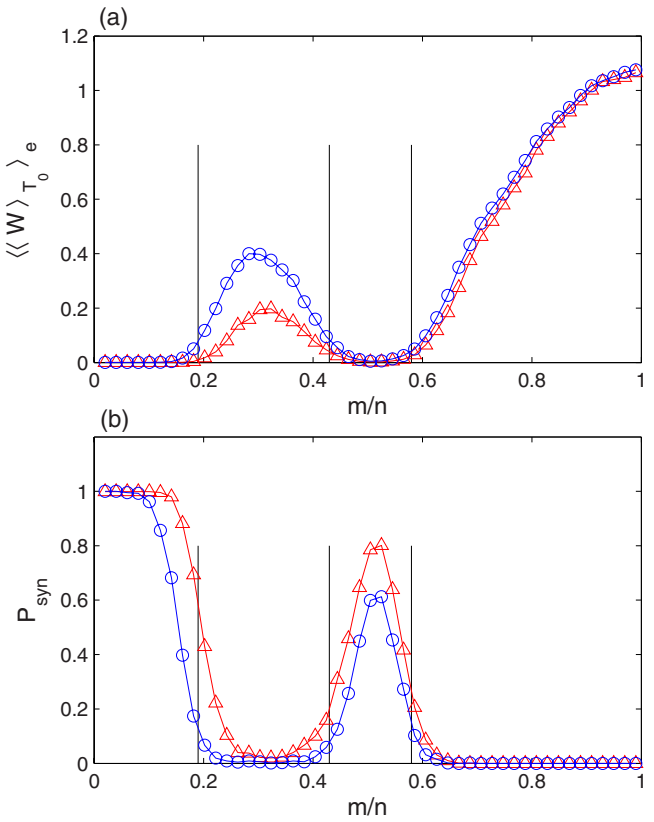

FIG. 6. (Color online) For a cluster oscillator network with parameters $N=200$, $M=2$, $p=0.2$, (a) $\langle\langle W\rangle_{T_0}\rangle_e$ vs m/n and (b) P_{syn} vs m/n. Circles and triangles indicate cases with bidirectional and directional intercluster connections, respectively. Simulation parameters are $T_0=10^4$ and $\delta=0.005$. The vertical lines indicating the boundaries are determined by $\lambda_2=K_1/\epsilon=0.5$. Each data point is the average of 700 realizations. The data for this figure were obtained with 15 Pentium-IV 2.80 GHz CPUs for about 2 months.

evidence for the existence of this behavior. For instance, we have chosen for each oscillator, when isolated, the Rössler dynamics $d\mathbf{x}/dt=\mathbf{F}(\mathbf{x})$, where $\mathbf{x}=[x,y,z]^T$, $\mathbf{F}(\mathbf{x})=[-(y+z),x+0.2y,0.2+z(x-9)]^T$, $\epsilon=0.4$, and $\mathbf{H}(\mathbf{x})=[x,0,0]^T$. Numerically, we find $K_1=0.2$ and $K_2=4.62$. Since the Rössler system can have desynchronization bursts, it is necessary to characterize the synchronization in a statistical way. In particular, we define

$$W(t)=\langle|x(t)-\langle x(t)\rangle|\rangle$$

as the fluctuation width of the system at time t, where $\langle\cdot\rangle$ denotes average over all nodes in the network. The ensemble and time averages of the fluctuation width $\langle\langle W\rangle_{T_0}\rangle_e$ can be an indicator of the degree of synchronization, i.e., if the system is synchronized, $\langle\langle W\rangle_{T_0}\rangle_e\approx 0$, and if not, $\langle\langle W\rangle_{T_0}\rangle_e$ may assume some large value. Figure 6(a) shows $\langle\langle W\rangle_{T_0}\rangle_e$ versus m/n for both the bidirectional and directional intercluster coupling cases. When m is small ($m/n<0.2$), $\langle\langle W\rangle_{T_0}\rangle_e$ is small and the system is synchronized. As m is increased ($m/n=0.3$), $\langle\langle W\rangle_{T_0}\rangle_e$ becomes large and desynchronization occurs. As m increases further ($m/n=0.5$), the fluctuation width reduces and the system becomes synchronized again, and for $m/n>0.6$, the network loses its synchronizability. The probability of synchronization, P_{syn}, defined as the probability that $W(t)$ is smaller than a small number δ at all time steps during a time interval T_0 in the steady state, can also be used to characterize the synchronizability. Practically, P_{syn} can be calculated by the ensemble average, i.e., the ratio of the number of synchronized cases over the total number of network realizations. Figure 6(b) shows P_{syn} vs m/n. The alternating synchronization phenomena is apparent, as predicted.

V. DISCUSSIONS

In this paper, motivated by the problem of tissue organization and intercellular communication in biology, we have studied the synchronizability of a class of clustered networks where each cluster contains a regular subnetwork. Our finding is that the network synchronizability exhibits an alternating, highly nonmonotonic behavior as the number of intracluster links (gap junctions in a biological network) changes. Although speculative, the results may suggest that the synchronized function of organs in the face of perturbation may be controlled by the ability of individual cells to vary the number of gap junctions expressed on the membrane, which has been observed in variations in gap junctional intercellular communication and connexion expression in fibroblasts derived from keloid and hypertrophic scars [27–29].

Using more biophysically detailed dynamical models for simulation of synchronous dynamics is an interesting problem. However, a detailed model that can satisfactorily treats the actual dynamical interactions in intercellular communication is beyond the scope of present research. Our goal in this paper has thus been to understand the synchronizability of the network, as synchronization is an important factor determining intercellular communications. The main advantage of the synchronizability analysis is that it allows us to draw quite general conclusions about the ability for nodes in the network to be synchronized. The key theoretical tool required for the analysis is spectral properties of the coupling matrix of the underlying network. We wish to emphasize that, although the synchronizability analysis can yield qualitative information about the likelihood for the network to achieve synchronization, it is not able to yield information about the detailed dynamical process that leads to synchronization. Because of this limitation, making the individual-node dynamics more "biological" is not very helpful from the standpoint of spectral analysis. In fact, insofar as the dynamics are oscillatory and somewhat random, we expect them to produce synchronization phenomena consistent with the predictions from the synchronizability analysis. That is why we have chosen the chaotic Rössler oscillator as a proper model for actual simulation of the synchronization dynamics. Indeed, the results from such numerical

computations agree, qualitatively, with the theoretical predictions based on spectral analysis.

Time delays of the interaction along the long-range links are important and relevant to the biological system. However, as discussed above, our synchronizability analysis is not designed to deal with time delays. This should be an interesting topic for future explorations.

ACKNOWLEDGMENTS

This work was supported by an ASU-UA Collaborative Program on Biomedical Research, by AFOSR under Grant No. FA9550-07-1-0045, by NSF under Grant No. ITR-0312131, and by ONR through WVHTC (West Virginia High Technology Consortium Foundation).

[1] L. F. Lago-Fernandez, R. Huerta, F. Corbacho, and J. A. Siguenza, Phys. Rev. Lett. **84**, 2758 (2000); M. Barahona and L. M. Pecora, *ibid.* **89**, 054101 (2002); X. F. Wang and G. Chen, Int. J. Bifurcation Chaos Appl. Sci. Eng. **12**, 187 (2002); S. Jalan and R. E. Amritkar, Phys. Rev. Lett. **90**, 014101 (2003).

[2] T. Nishikawa, A. E. Motter, Y.-C. Lai, and F. C. Hoppensteadt, Phys. Rev. Lett. **91**, 014101 (2003).

[3] M. Chavez, D.-U. Hwang, A. Amann, H. G. E. Hentschel, and S. Boccaletti, Phys. Rev. Lett. **94**, 218701 (2005); C. Zhou, A. E. Motter, and J. Kurths, *ibid.* **96**, 034101 (2006); X.-G. Wang, Y.-C. Lai, and C. H. Lai, Phys. Rev. E **75**, 056205 (2007).

[4] M. Zhao, T. Zhou, B.-H. Wang, and W.-X. Wang, Phys. Rev. E **72**, 057102 (2005); L. Donetti, P. I. Hurtado, and M. A. Muñoz, Phys. Rev. Lett. **95**, 188701 (2005); S. Boccaletti, D.-U. Hwang, M. Chavez, A. Amann, J. Kurths, and L. M. Pecora, Phys. Rev. E **74**, 016102 (2006); J. G. Restrepo, E. Ott, and B. R. Hunt, Phys. Rev. Lett. **97**, 094102 (2006).

[5] E. Oh, K. Rho, H. Hong, and B. Kahng, Phys. Rev. E **72**, 047101 (2005).

[6] K. Park, Y.-C. Lai, S. Gupte, and J.-W. Kim, Chaos **6**, 015105 (2006).

[7] L. Huang, K. Park, Y.-C. Lai, L. Yang, and K. Yang, Phys. Rev. Lett. **97**, 164101 (2006).

[8] P. Erdös and A. Rényi, Publ. Math. Inst. Hung. Acad. Sci. **5**, 17 (1960).

[9] D. J. Watts and S. H. Strogatz, Nature (London) **393**, 440 (1998).

[10] A.-L. Barabási and R. Albert, Science **286**, 509 (1999).

[11] Y. Ho *et al.*, Nature (London) **415**, 180 (2002).

[12] V. Spirin and L. A. Mirny, Proc. Natl. Acad. Sci. U.S.A. **100**, 12123 (2003).

[13] G. Palla, I. Derényi, I. Farkas, and T. Vicsek, Nature (London) **435**, 814 (2005).

[14] E. Ravasz, A. L. Somera, D. A. Mongru, Z. Oltvai, and A.-L. Barabási, Science **297**, 1551 (2002).

[15] D. J. Watts, P. S. Dodds, and M. E. J. Newman, Science **296**, 1302 (2002); R. Milo, S. Shen-Orr, S. Itzkovitz, N. Kashtan, D. Chklovskii, and U. Alon, *ibid.* **298**, 824 (2002); K. A. Eriksen, I. Simonsen, S. Maslov, and K. Sneppen, Phys. Rev. Lett. **90**, 148701 (2003); A. E. Motter, T. Nishikawa, and Y.-C. Lai, Phys. Rev. E **68**, 036105 (2003); E. Oh, K. Rho, H. Hong, and B. Kahng, *ibid.* **72**, 047101 (2005).

[16] E. Yeger-Lotem, S. Sattath, N. Kashtan, S. Itzkovitz, R. Milo, R. Y. Pinter, U. Alon, and H. Margalit, Proc. Natl. Acad. Sci. U.S.A. **101**, 5934 (2004).

[17] S.-H. Yook, Z. N. Oltvai, and A. L. Barabási, Proteomics **4**, 928 (2004).

[18] B. Grunenfelder and E. A. Winzeler, Nat. Rev. Genet. **3**, 653 (2002).

[19] S. Li *et al.*, Science **303**, 540 (2004).

[20] J.-D. J. Han *et al.*, Nature (London) **430**, 88 (2004).

[21] R. A. Gatenby and B. R. Frieden, Cancer Res. **62**, 3675 (2002); R. A. Gatenby and T. L. Vincent, *ibid.* **63**, 6212 (2003); R. A. Gatenby and R. J. Gillies, Nat. Rev. Cancer **4**, 891 (2004); R. A. Gatenby and B. R. Frieden, Bull. Math. Biol. **69**, 635 (2006).

[22] For example, a human liver typically contains 10^{12} cells and has the length scale of about 15 cm, which is equivalent to about 10^5 cell diameters.

[23] M. Lamboley, P. Pittet, M. Koenigsberger, R. Sauser, J. L. Beny, and J. J. Meister, Cell Calcium **37**, 311 (2005).

[24] J. Jost and M. P. Joy, Phys. Rev. E **65**, 016201 (2001).

[25] L. M. Pecora and T. L. Carroll, Phys. Rev. Lett. **80**, 2109 (1998).

[26] Let $\mathbf{b}=[1\ 1\cdots]^T$, $(\mathbf{b}^T\mathbf{G}^T)_i=\Sigma_{j=1}^N G_{ij}=0$, thus $\mathbf{b}^T\mathbf{G}^T=[0\ 0\cdots]$. Therefore, $\mathbf{b}^T\mathbf{G}^T\mathbf{e}_i=\lambda_i\Sigma_j^N e_{i,j}=0$. If $\lambda_i\neq 0$, then $\Sigma_j^N e_{i,j}=0$ (λ_i and $e_{i,j}$ could be complex).

[27] D. S. Friend and N. B. Gilula, J. Cell Biol. **53**, 758 (1972).

[28] N. DePaola, P. F. Davies, W. F. Pritchard, L. Florez, N. Harbeck, and D. C. Polacek, Proc. Natl. Acad. Sci. U.S.A. **96**, 3154 (1999).

[29] F. Lu, J. Gao, R. Ogawa, and H. Hyakusoku, Plast. Reconstr. Surg. **119**, 844 (2007).